JOURNAL OF APPLIED CRYSTALLOGRAPHY

Volume 56 (2023)

Supporting information for article:

Strain generated by the stacking faults in epitaxial SrO(SrTiO3)N Ruddlesden-Popper superlattices

Guillaume Saint-Girons, Clarisse Furgeaud, Ludovic Largeau, Alexandre Danescu, Romain Bachelet and Mohamed Bouras

S1. Sample growth

The results of the characterizations of the reference sample are displayed in Fig.S1.

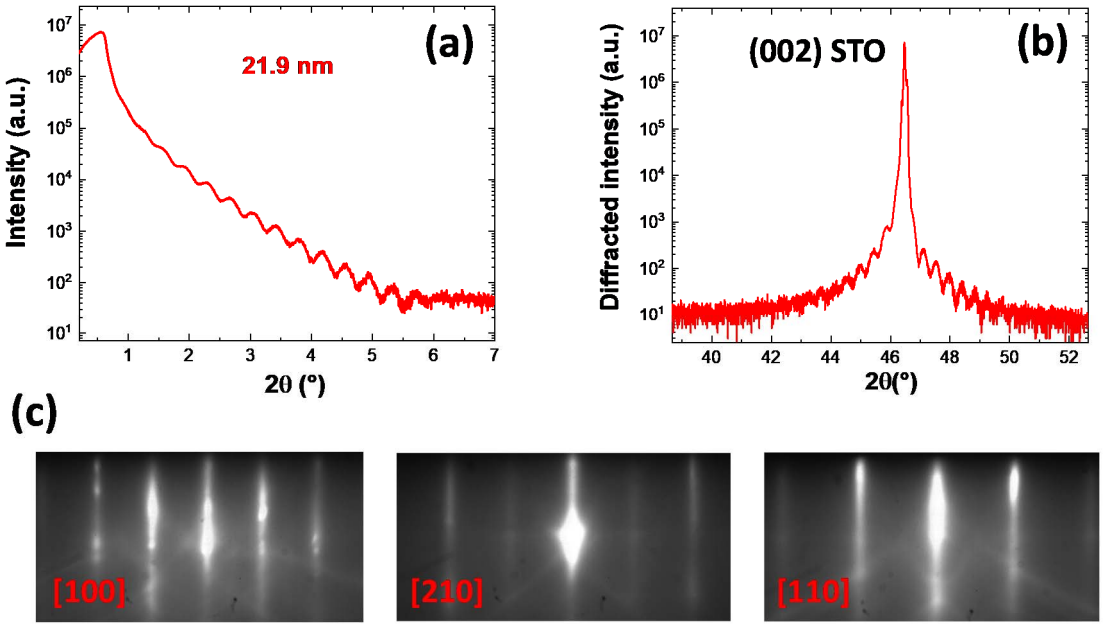

Figure S1 (a) XRR spectrum of the reference sample. (b) XRD diffractogram of the reference sample recorded around the (002) reflexion of the STO substrate. (c) RHEED patterns recorded at the end of the growth of the reference sample.

The thickness of the reference sample (21.9 nm) was deduced from the period of the fringes in the X-ray reflectivity (XRR) spectrum. This corresponds to a growth rate of 1.4 monolayer (ML)/min (growth duration : 40 min). In the X-ray diffraction (XRD) diffractogram of Fig.S1(b), the STO layer reflexion cannot be distinguished from that of the substrate, showing that the layer composition is nearly stoichiometric. This is confirmed by the RHEED patterns displayed in Fig.S1(c), where no (respectively very weak) half-order lines are detected on the [100] and [110] (respectively [210]) azimuths.[1]

The growth sequence used to fabricate the RP sample is displayed in Fig.S2.

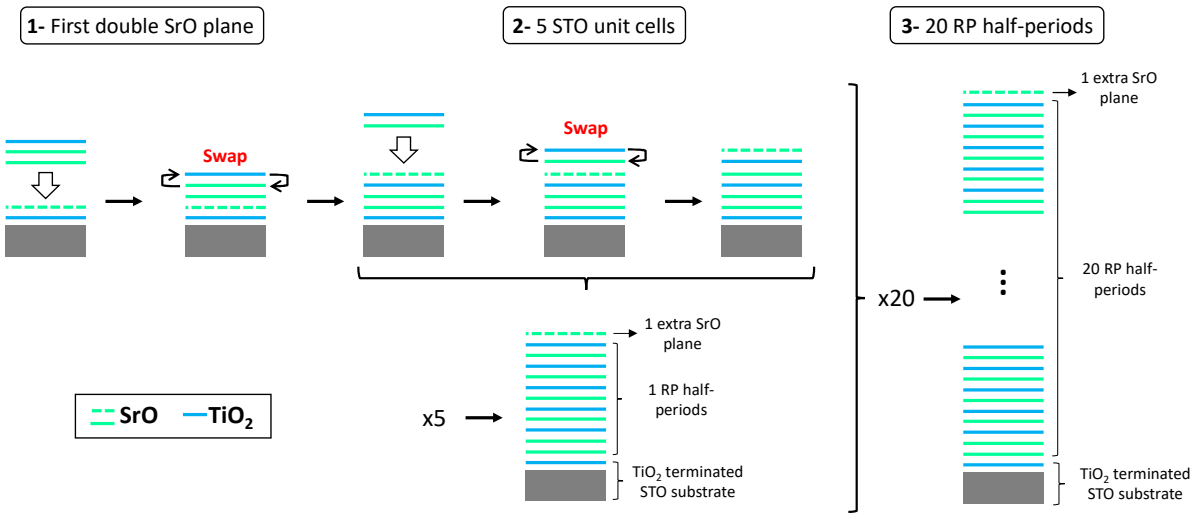

Figure S2 Growth sequence used to fabricate the RP sample.

It relies on the swapping mechanism described in Ref.[2] and [3]: during the deposition of a TiO_2 plane on a double SrO plane, it is energetically favorable that the growing TiO_2 plane swaps with the last SrO plane : a TiO_2/SrO/SrO growth sequence spontaneously leads to a SrO/TiO_2/SrO stack. RP layers grown by using TiO_2/SrO swap sequences present improved structural order as compared to those grown by directly using the RP atomic layer sequence. Thus, the growth sequence is as follows:

1-Formation of the first double SrO plane: a SrO atomic plane is deposited on a TiO_2 terminated STO substrate. Then, two SrO atomic planes and one TiO_2 plane are added. This last TiO_2 plane swaps with the last SrO plane to form a SrO/TiO_2/SrO/SrO stack on the TiO_2 terminated STO substrate.

2-Formation of the first RP half-period: five SrO/TiO_2 double planes are deposited on the stack obtained after step 1. Each time, the last TiO_2/SrO stack at the growth front swaps to form a SrO/TiO_2 stack, leading to the formation of the first RP half-period (a double SrO plane and five STO unit cells) on the TiO_2-terminated STO substrate. An extra SrO plane remains on the growth front and is present on the surface above the RP half-period.

3-Growth of 20 RP half-periods: the SrO+5x(SrO+TiO2) deposition sequence is repeated 20 times to form the 20 RP half-periods. An extra SrO plane remains on the growth front and is present on the sample surface at the end of the growth.

The global growth sequence applied to fabricate the sample thus reads:

(1 SrO atomic plane) + 20x[(1 SrO atomic plane)+5x((1 SrO atomic plane)+(1 TiO_2 atomic plane))]

S2. Superlattice description of the RP stack

We use the superlattice description of the RP stack sketched in Fig.S3 to interpret the XRD patterns shown in the manuscript.

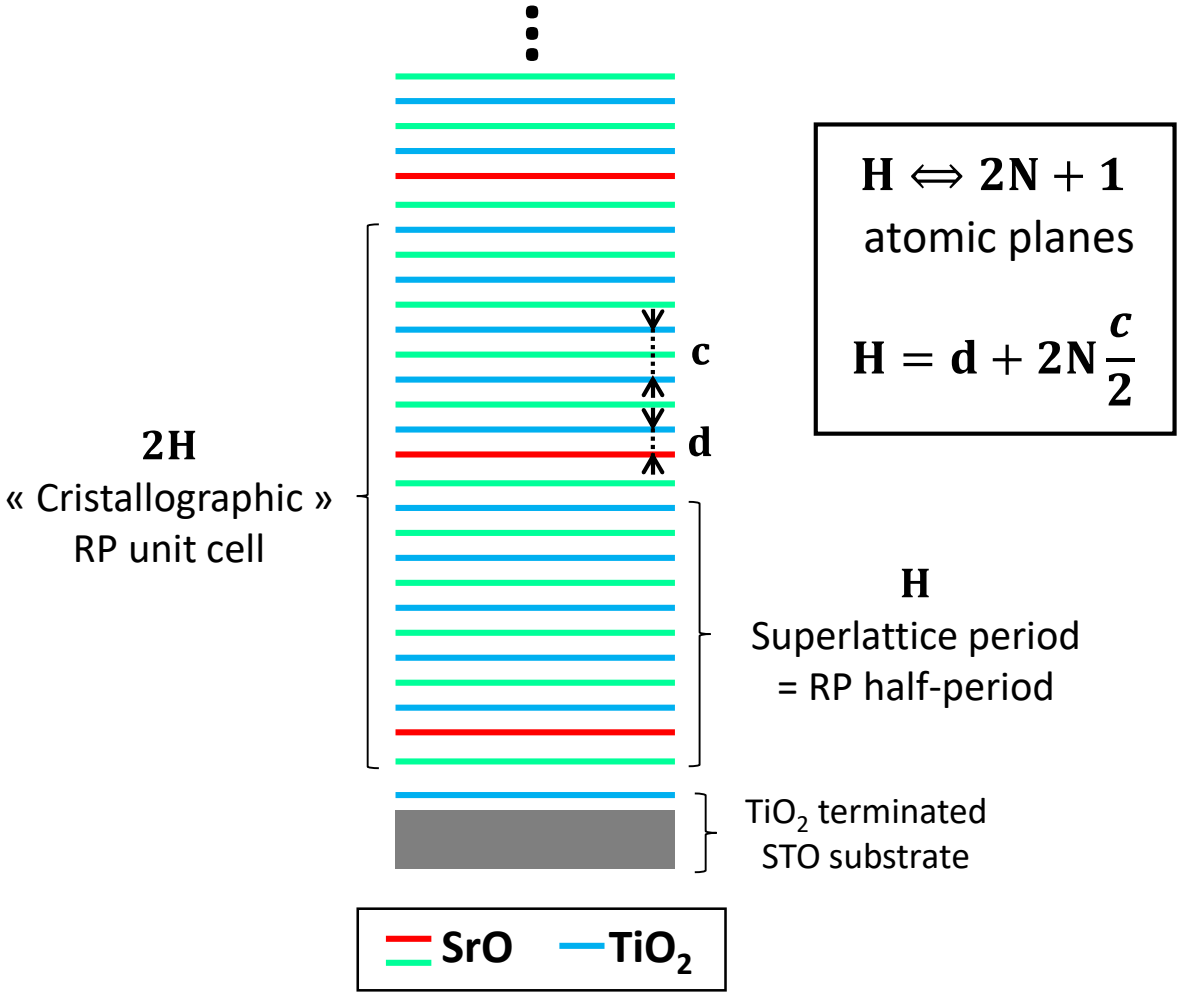

Figure S3 RP[5] structure described as a superlattice of period H comprising 2N + 1 atomic planes.

d is the SrO-SrO interplanar distance, and c is the STO unit cell, as defined in the manuscript. The RP structure is described as a superlattice of period $H = d + 2N\frac{c}{2}$ consisting of $2N + 1$ atomic planes. The superlattice period corresponds to half the "crystallographic" RP unit cell. Note that this description does not account for the in-plane shift of the lattice of half the STO unit cell along the [110] direction at each IP-SF, and fails for this reason to describe the extinction of the odd-order RP reflections. However, it describes accurately the atomic arrangement along OP.

S3. Analysis of the STEM-HAADF images

The STEM-HAADF image of the **RP_0** region is displayed in Fig. S4

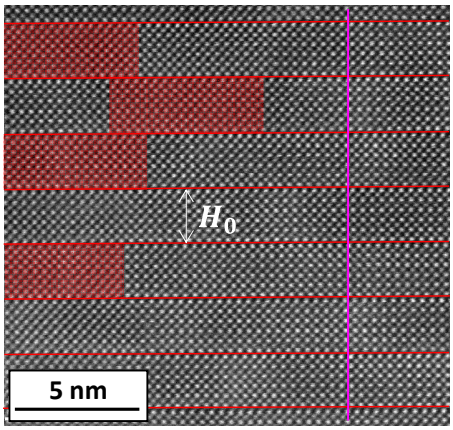

Figure S4 STEM-HAADF image of the RP_0 region.

Intensity profiles were recorded along the pink lines indicated in the figure to measure H_0 and c. This cutline is far from the regions where OP-SF lying perpendicular to the viewing direction are detected, to prevent the measurement from being disturbed by these defect. To limit measurement uncertainty, the distance corresponding to $7H_0$was measured and divided by 7. For c, we performed 7 measurements of the 5c distance, and averaged the results. This leads to $H_0 = 22.16 \pm 0.015$ Å and $c = 3.921 \pm 0.008$ Å.

The STEM-HAADF image of the $IG_{1/3}/RP_{1/3}$ regions is displayed in Fig. S5

$$32 \times \frac{\bar{c}^{RP}_{1/3}}{2} = 63.3 \pm 0.15 \text{ Å} \Longrightarrow \bar{c}^{RP}_{1/3} = 3.96 \pm 0.01 \text{ Å}$$

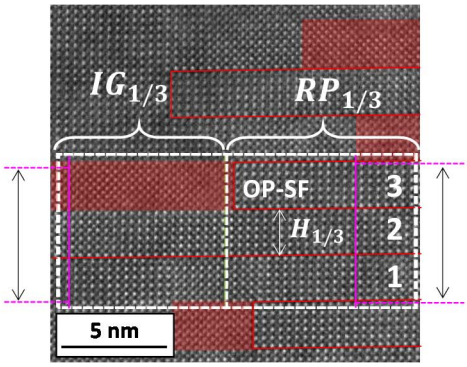

$$3 \times H_{1/3} = 65.5 \pm 0.15 \text{ Å} \Longrightarrow H_{1/3} = 21.83 \pm 0.05 \text{ Å}$$

Figure S5 STEM-HAADF image of the $IG_{1/3}/RP_{1/3}$ regions.

Intensity profiles were recorded along the pink lines indicated in the figure to measure $H_{1/3}$ and $\bar{c}^{RP}_{1/3}$. The uncertainty corresponds to the pixel size.

S4. Shoulders in the diffraction pattern : RP half-period modulation vs thickness fringes

The shoulders on the X-ray diffractograms of Fig.3, which we attribute to RP half-period modulation due to OP-SF, look somewhat similar to thickness fringes. We show here however that thickness fringes cannot explain the shape of these diffractograms. Fig.S6 compares the latter with that calculated for a perfect RP[5] lattice with a thickness corresponding to 20 RP half-periods, free of any OP-SF.

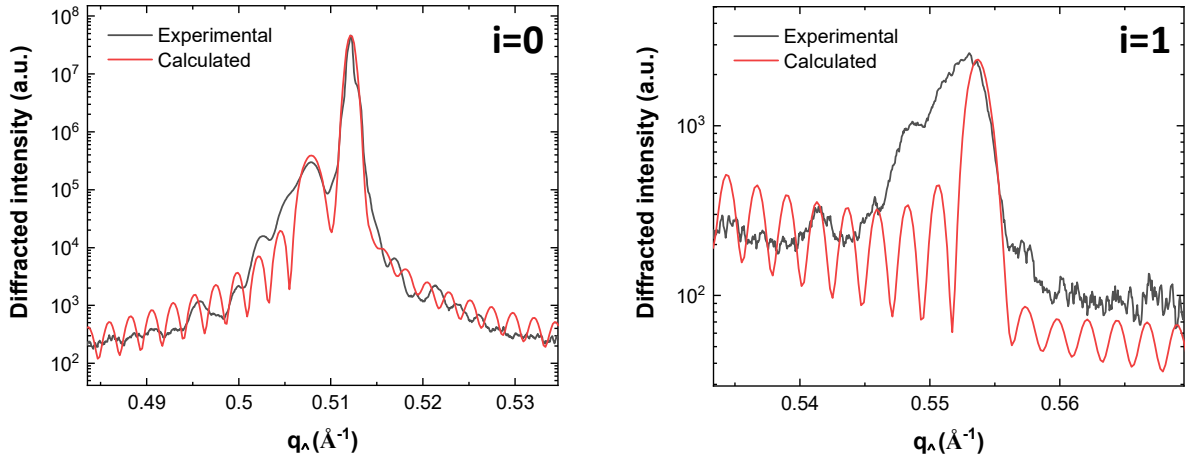

Figure S6 Experimental diffractogram of the RP[5] sample (black) compared to that calculated for a perfect RP[5] of thickness corresponding to 20 RP half-periods (red). Left : 0th order peak and right : 1st order satellite.

The perfect RP[5] diffractogram (black line in Fig.S7) was calculated as

$I(q) = F \times F^*(q) + sub(q)$, with $F = F_{UC} \sum_{\alpha=0}^{N_H-1} e^{-2j\pi H\alpha}$ the structure factor of the perfect RP, and

$$sub(q) = A\left[\mu \frac{2}{\pi} \frac{w}{4(q-q_c)^2 + w^2} + (1-\mu)\frac{\sqrt{4\ln(2)}}{w\sqrt{\pi}} \exp\left(-\frac{4\ln(2)}{w^2}(q-q_c)^2\right)\right]$$

a pseudo-voigt function describing the substrate contribution. F_{UC} is the structure factor of a RP half unit cell, $N_H = 20$ is the number of RP half-period of the sample, and H is the RP half-period, set for this calculation to 21.66 Å to best match the experimental data. $I(q)$ was normalized and corrected from a constant baseline to ease the comparison with the calculated data. The positions of the calculated thickness fringes are quite close to that of the experimental shoulders attributed to RP half-period modulation, as expected since the layer thickness is an integer number of RP half-periods. There is however a clear discrepancy between the experimental and calculated peak positions. This discrepancy comes from the fact that the modulation mechanism described in the manuscript produces a dispersion in the period that is described by the perfect RP[5] model. Moreover, the experimental shoulder intensities do not correspond to what is expected for thickness fringes, which reinforces the statement that the latter are not at the origin of the shape of the diffractogram. Hybrid reflections from multiple X-ray scattering, reported in Ref.[4] for oxide thin films, may cause a modulation of the thickness fringes that may lead to diffractogram shape similar to that of Fig.S6. Such effect would however be dependent upon the azimuthal angle ϕ (angle defined in the inset of Fig.S7). To rule out this hypothesis, we compare in Fig.S7 radial scans recorder on the sample at different values of ϕ.

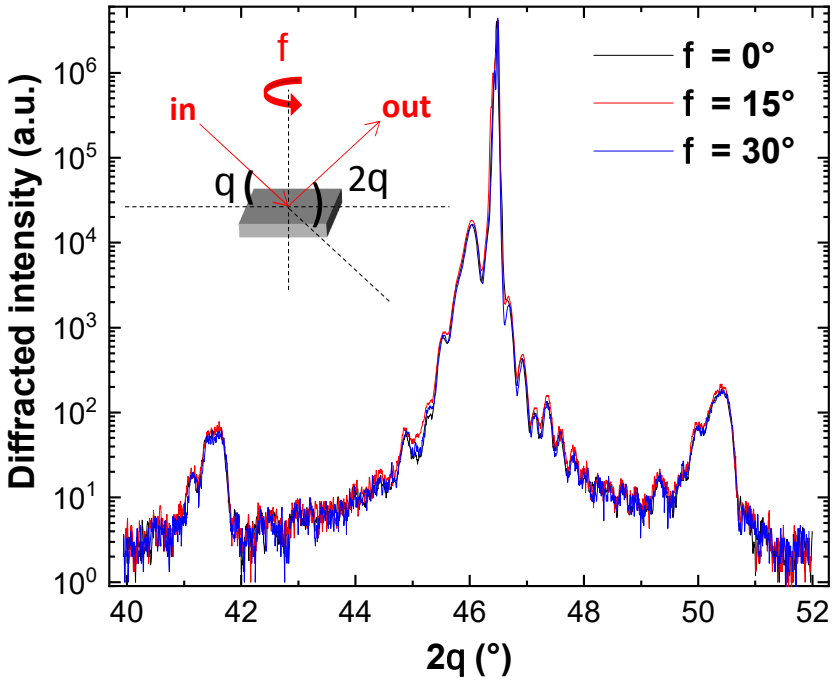

Figure S7 Radial scans recorded on the RP[5] sample for $\phi = 0°$ (incident beam direction parallel to the <100> substrate edge), $\phi = 15°$ and $\phi = 30°$

These scans have very similar shapes, discarding the hypothesis of thickness fringes intensity modulation caused by multiple X-ray scattering, and decisively supporting the statement that the shoulders are caused by RP half-period modulation caused by the OP-SF.

S5. References

[1] M. Razaghi Pey Ghaleh, M. d'Esperonnat, C. Botella, S. Cueff, R. Bachelet and G. Saint-Girons, Sensitive RHEED signature of Ti-excess enabling enhanced cationic composition control during the molecular beam epitaxy of SrTiO3 based solid solutions, CrystEngComm **23**, 2269 (2021)

[2] Y. F. Nie, Y. Zhu, C.-H. Lee, L. F. Kourkoutis, J. A. Mundy, J. Junquera, P. Ghosez, D. J. Baek, S. Sung, X. X. Xi *et al.*, Atomically precise interfaces from non-stoichiometric deposition, Nat. Commun. **5**, 4530 (2014)

[3] J. H. Lee, G. Luo, I. C. Tung, S. H. Chang, Z. Luo, M. Malshe, M. Gadre, A. Bhattacharya, S. M. Nakhmanson, J. A. Eastman *et al.*, Dynamic layer rearrangement during growth of layered oxide films by molecular beam epitaxy, Nat. Mater. **13**, 879 (2014)

[4]E. H. Smith, P.D.C. King, A. Soukiassian, D.G. Ast and D.G. Schlom, Hybrid reflections from multiple x-ray scattering in epitaxial oxide films. Appl. Phys. Lett. **111**, 131903 (2017)